



Comparative study between green and red algae in the control of corrosion and deposition of scale in water systems

Essam Khamis^a, Essam El-Rafey^b, Ashraf Moustafa Abdel Gaber^c, Ahmed Hefnawy^b, Nihal Galal El-Din Shams El-Din^{d,*}, Mayssa Salah El-Din Esmail Ahmed^e

^aFaculty of Science, Chemistry Department, Alexandria University, Ibrahimia, P.O. Box 426, Alexandria 21321, Egypt, Tel. +20 1222168919; email: essam_khamis@mucsat.sci.eg

^bMaterial Science Department, Institute of Graduate Studies and Research, Alexandria University, Alexandria, Egypt, Tel. +20 1222168919; emails: igsrdean@gmail.com (E. El-Rafey), hefn5@yahoo.com (A. Hefnawy)

^cFaculty of Science, Department of Chemistry, Beirut Arab University, Beirut, Lebanon, Tel. +20 34288078; email: ashrafmoustafa@yahoo.com

^dMarine Environment Department, National Institute of Fisheries and Aquatic Research, Kayet Bay El Anfouchy, Alexandria, Egypt, Tel. +20 1224267840; email: nihalshamseldin@yahoo.com

^eCentral Lab and Research, Quality Control and Environment Department, Alexandria Water Company, Alexandria, Egypt, Tel. +20 1229732057; email: joe3_3@yahoo.com

Received 30 April 2015; Accepted 18 December 2015

ABSTRACT

Scale deposition and corrosion have become a nightmare for any oil and gas operations. The antiscalant properties of the green algal (*Ulva compressa*) and the red algal (*Pterocladia capillacea*) extracts were studied using conductivity, electrochemical impedance spectroscopy (EIS), and chronoamperometry techniques in conjunction with microscopic and infrared examinations. The corrosion inhibitive characteristics were investigated using EIS and potentiodynamic polarization measurements. Mineral scales were deposited from the brine solution by cathodic polarization of the steel surface at -0.9 V (vs. SCE). Potentiodynamic polarization curves indicated that the green algal (*U. compressa*) and the red algal (*P. capillacea*) extracts inhibit the corrosion of steel by controlling the cathodic oxygen reduction process.

Keywords: Scales; Corrosion; Algal extracts; Brine solution; EIS; Chronoamperometry; Optical microscope examination; SEM; IR

1. Introduction

The use of chemical compounds in a variety of applications is conditioned by environmental and health concerns. Accordingly, during the last years, industrial requirements for chemical compounds refer not only to their efficacy but to safety as well. The requisites for these compounds should focus on non-muta-

genic, non-carcinogenic products with characteristics more environmentally acceptable than systems currently in use [1,2].

A number of antiscalants are commercially available and new formulations are continuously being developed and tested for a variety of scaling species [3–5]. Moreover, many corrosion inhibitors have been used in cooling water systems [6,7]. Particularly, chromates and many other heavy metals were the

*Corresponding author.

standard corrosion inhibitors of choice, because of a long history of successful commercial usage and their excellent effectiveness over a wide range of conditions [8,9]. However, the popularity of inhibitors containing heavy metals is diminishing, because of the concern over their toxic effects on aquatic and possibly animal life [10].

Therefore, the hazardous effects of most synthetic corrosion inhibitors are the motivation for the use of natural products. Recently, plant extracts have become important as sustainable, environmentally acceptable, readily available, and renewable source for a wide range of needed inhibitors. Plant extracts are viewed as an incredibly rich source of naturally synthesized chemical compounds that can be extracted by simple procedures with low cost. Various natural products were used as corrosion inhibitors in different applications [11–13]. The obtained data showed that plant extracts could serve as effective environmentally friendly “green” corrosion inhibitors.

However, Egyptian marine seaweeds were currently used to solve many problems in many different domains. Mansour et al. [14] developed a new anticorrosive coating containing green alga *Ulva lactuca* as natural inhibitor for preventing marine corrosion of steel.

On the other hand, *Ulva compressa* (*U. compressa*) formerly known as *Enteromorpha compressa* and *Pterocladia capillacea* (*P. capillacea*) formerly known as *Pterocladia capillacea* [15] are the most common algae in the Mediterranean coastal zone [16,17]. The principal cell wall polysaccharides in green seaweeds are ulvans, those in red seaweeds are agarans and carrageenans [18]. The polysaccharide content of seaweed is very high, accounting for more than 50% of the dry weight [19]. Ulvans represent 8–29% of the green algal dry weight. Carrageenans are one of the major constituents of red seaweed cell walls representing 30–75% of the algal dry weight [20]. The two species were used as antimicrobial and anticancer agents, but were not investigated as anticorrosion or antiscalant agents before.

The aim of this study was to investigate *U. compressa* and *P. capillacea* algal extracts as a novel environmentally friendly anticorrosion and antiscalant for CaCO_3 calcareous deposits on steel in an alkaline CaCl_2 brine solution using electrochemical impedance spectroscopy (EIS), chronoamperometry techniques, conductivity measurements, and microscopic and infrared examinations.

2. Materials and methods

2.1. Sample collection

Macroalgal samples were collected at the depths (0.5–1 m) during winter (December, 2011) at the beach

located along the western head of Abu-Qir Bay between longitudes $30^\circ 07' \text{ E}$ and latitude $31^\circ 33' \text{ N}$, (Fig. 1). The two macroalgae were handpicked from their bases [21], scraping the substrata on which they were adhered. Then, they were washed with seawater at the sampling site to remove the remained adhered sediments, separated in polyethylene bags, and stored under refrigeration at 4°C . Quick rinsing of the algae with tap water was carried out in the laboratory on the same day to get rid of the remaining impurities and epiphytes. Herbarium sheets with a preliminary identification of the two algal species were done and/ or preserved in 4% formalin. Microscopic identification of the two species was carried out according to [22].

The first species *U. compressa* (Linnaeus) Nees, belongs to the class Chlorophyceae; order Ulvales; family Ulvaceae. The second species *P. capillacea* (S.G. Gmelin) Santelices and Hommersand [15], belongs to the class Rhodophyceae; order Gelidiales; family Pterocladaceae.

2.2. Solution preparation

Distilled water and analytical reagent grade NaCl , NaHCO_3 , Na_2CO_3 , Na_2SO_4 , and CaCl_2 were used for preparing solutions. The CaCl_2 brine solution was prepared to a concentration of 0.7 M NaCl , 0.0025 M NaHCO_3 , 0.028 M Na_2SO_4 , and 0.01 M CaCl_2 [14].

Stock solutions of algal extracts were obtained by addition of 500 mL of analytical grade methanol (98%) to 50 g of wet tissue and left for 1 h at 37°C during which the samples were mixed slowly each 10 min.

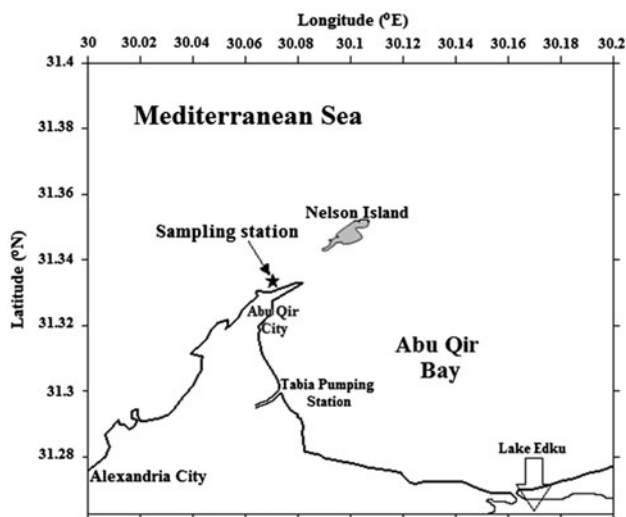


Fig. 1. The study area and sampling station during winter (2011).

The extracts were then filtered and the filtrate was collected and stored at -20°C .

2.3. Conductivity test

The test setup as described previously [20] consisted of a glass container, mechanical stirrer and conductivity sensor of a traceable conductivity meter. The setup was carefully cleaned by 1 M H_2SO_4 and distilled water to remove all traces of deposits, which could become a source of crystal nuclei. Prior to each experiment, 5 mL of 0.1 M CaCl_2 solution is added to an appropriate volume of the stock solution of *U. compressa* and *P. capillacea* algal extract; then the mixture was completed to 100 mL with distilled water. The conductivity of the stirred solution was measured by titrating with 0.1 M Na_2CO_3 . The titrating solution was added in portions of 0.2 mL each. Measurements were done at $25.0 \pm 0.1^{\circ}\text{C}$.

2.4. Electrochemical techniques

The electrochemical measurements were carried out in a three-electrode mode; platinum sheet and saturated calomel electrodes were used as counter and reference electrodes. The material used for constructing the working electrode was steel that had the following chemical composition (wt%): C, 0.21; S, 0.04; Mn, 2.5; P, 0.04; Si, 0.35; balance Fe. The steel was encapsulated in epoxy resin in such a way that only one surface was left uncovered. The exposed area (0.785 cm^2) was mechanically abraded with a series of emery papers of variable grades, starting with a coarse one and proceeding in steps to the finest (600) grade. The samples were then washed thoroughly with distilled water, followed with A.R. ethanol and finally with distilled water, just before insertion in the cell.

Chronoamperometry and electrochemical impedance measurements were achieved using a GAMRY instrument (G750).

Chronoamperometry curves were carried out by polarizing the steel electrode to -0.9 V (vs. SCE) in test solution for a total of 20 h. Thus, the current passing through the steel electrode, during calcareous deposits, was recorded with respect to time. The electrochemical impedance spectra (EIS) were made at an open circuit potential in a renewed solution. The frequency range for EIS measurements was $0.1\text{--}5 \times 10^3\text{ Hz}$ with applied potential signal amplitude of 10 mV. Before polarization and EIS measurements, the working electrode was left for 30 min to attain the open circuit potential in the used solution.

Polarization curve measurements were made by polarizing the working electrode from -250 mV cathodically to $+250\text{ mV}$ anodically with respect to open circuit potential at a scan rate of 30 mV/min starting from cathodic potential (Ecorr -250 mV) going to anodic direction. All the measurements were made at $40.0 \pm 0.1^{\circ}\text{C}$ in solutions open to the atmosphere under unstirred conditions. To test the reliability and reproducibility of the measurements, duplicate experiments were performed in each case with the same conditions.

2.5. Microscopic examination

Optical micrographs ($40\times$) were taken with a Euro-mex optical microscope with color video camera that is connected to a personal computer.

Scanning electron microscope examinations were carried out using (JEOL JSM-5300 Scanning Microscope) with resolution of $10\text{--}20\text{ nm}$, after coating the electrode surface with a golden layer. The magnification at high vacuum mode are $15\times$ to $200,000\times$ and at low vacuum mode are $15\times$ to $50,000\times$. Acceleration voltages $0.5\text{--}30\text{ kV}$.

2.6. FTIR analysis

The FTIR spectra measurements of the solid sample were recorded by averaging 64 scans at a resolution of 4 cm^{-1} using a Perkin-Elmer FT.IR Spectrum BX system spectrometer in the spectral region between $4,000$ and 500 cm^{-1} using KBr pellet.

3. Results and discussion

3.1. Scale inhibition

3.1.1. Conductivity measurements

In order to test and evaluate the ability of a given substance to inhibit the scale formation Drela et al. [23] developed a rapid and simple chemical test based upon the solution conductivity measurements, while calcium carbonate is being precipitated from calcium chloride solution by addition of sodium carbonate. So, this method was used as the first step to test the efficiency of *U. compressa* and *P. capillacea* algal extract as scale inhibitor. Fig. 2 shows the variation of solution conductivity of CaCl_2 with the amount of sodium carbonate added in the presence or absence of different *U. compressa* and *P. capillacea* algal extract concentrations.

It is clear that the conductivity of the solution increased linearly with increasing the added amount

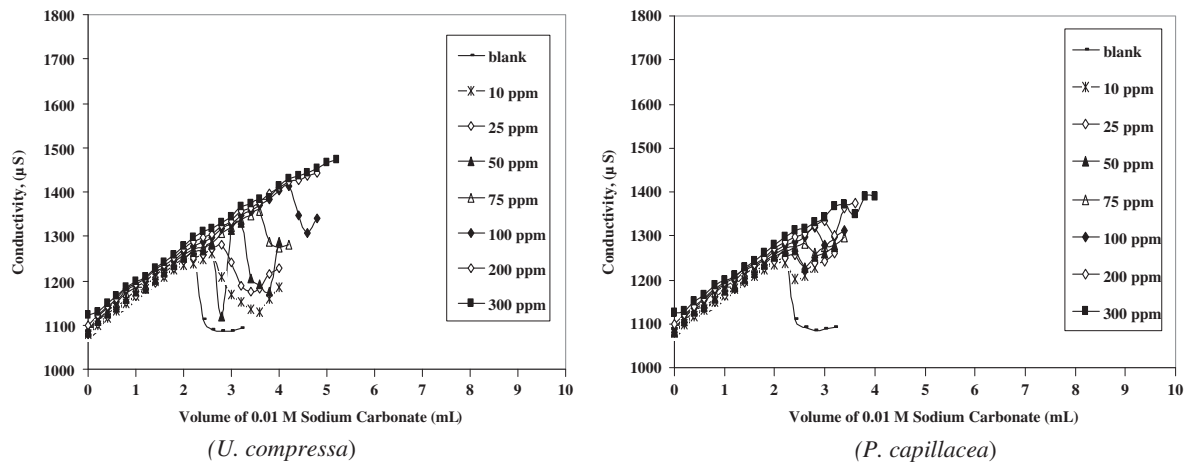


Fig. 2. Variation of conductivity of 0.1 M CaCl_2 solution in the absence or presence of different concentrations of algal extract with the volume of 0.1 M Na_2CO_3 at 25 °C.

of the sodium carbonate up to a certain point where the solution became supersaturated, and a rapid precipitation of CaCO_3 began, resulting in a decrease in conductivity. After complete precipitation, further addition of sodium carbonate produced more ions in the solution that increased the conductivity again. However, the figure revealed that increasing *U. compressa* and *P. capillacea* algal extract concentration shifted the maximum, after which precipitation occurred, to a higher amount of sodium carbonate. This indicated that the presence of *U. compressa* and *P. capillacea* algal extract impeded the supersaturation which may be attributed to the adsorption of the extracted molecules onto the active sites of the growing crystals, causing suspended solids to disperse and liquefy which reduced the rate of crystal growth [24]. The adsorption could take place via: (i) electrostatic attraction between the charged particles and the charged chemical constituents of the extract; (ii) a dipole-type interaction between unshared electrons pairs in the extracted molecules and growing particles; (iii) π -interaction with particles surfaces; and (iv) a combination of all of the above [25], where, they are matched with the experiments carried out by Abdel-Gaber et al. [11]. The inhibitive properties of algal extracts are largely dependent on the chemical constituents and cell wall composition of the algae [18–20]. It is clear that, the efficiency of *U. compressa* is higher than *P. capillacea* extracts.

3.1.2. Electrochemical techniques

3.1.2.1. Chronoamperometry measurements. Several investigators have used the Chronoamperometry technique to investigate scaling processes [26,27]. The current

passing through the electrode is recorded with respect to time, while the electrode is polarized at the diffusion limiting current of oxygen (c.a. -0.9 V vs SCE). It is well documented that the scales can be formed on metal surfaces under cathodic polarization. These scales cover the active surface area available for the electrochemical reactions and consequently reduce the current density [28]. Fig. 3(a) shows the chronoamperometry curve for polarized steel electrode in the CaCl_2 brine solution at 40 °C. As seen, the plot can be separated into three regions: nucleation, growth, and total coverage of the electrode surface. During the first stage, the initial current decrease is attributed to some decrease in the oxygen reduction rate, which is strongly dependent on the electrode pretreatment. The scaling process is initialized by increasing the local pH near the electrode surface by means of the reduction of the dissolved oxygen in brine solution according to the chemical equation:



The resulting hydroxide ions force few nuclei of CaCO_3 to begin on the electrode surface according to the chemical reaction:



In the second stage, the current decreased linearly, indicating that the nuclei already born were growing and occupied the surface, leaving some parts free. In the third stage, the current reached a limiting value of

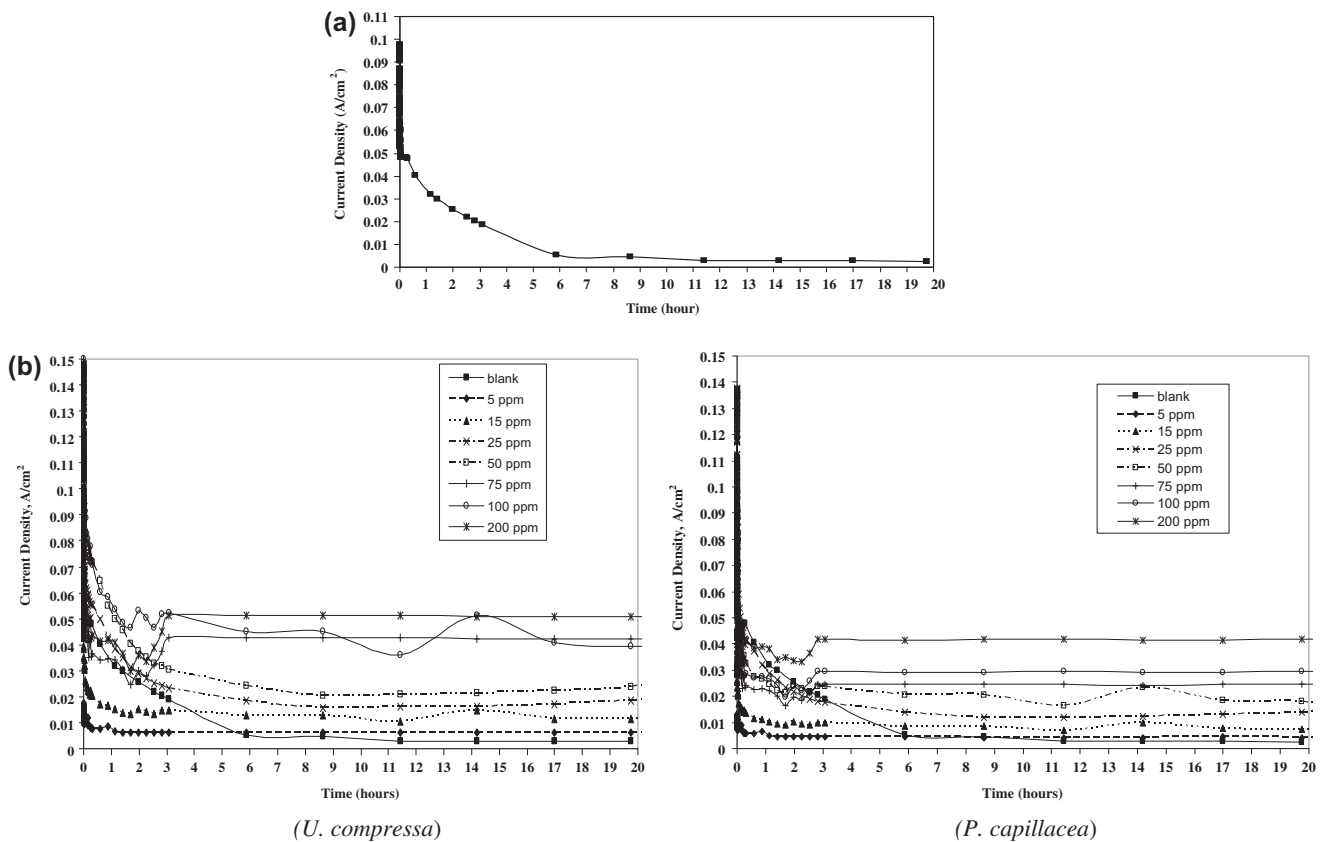


Fig. 3. (a) Chronoamperometry curve for polarized steel in the CaCl_2 brine solution at 40°C and (b) chronoamperometry curves for polarized steel electrode in the CaCl_2 brine solution in the absence or the presence of different concentrations of algal extract at 40°C .

$6.06 \times 10^{-4} \text{ A/cm}^2$ after 7 h, which defined practically the scaling time at which total coverage of the electrode surface was obtained. The low limiting current value suggests that the surface coverage was porous, since if it was completely blocked, the current would be zero.

Fig. 3(b) shows the chronoamperometry curves for polarized steel electrode in the CaCl_2 brine solution in the absence or presence of different *U. compressa* and *P. capillacea* algal extract concentrations at 40°C , respectively. It is clear that the addition of 5 ppm of the extract to the brine solution increased the nucleation time and decreased the growth rate that is described by the slope of the line representing the growth step. Higher concentrations of *U. compressa* and *P. capillacea* algal extract (75 and 100 ppm), respectively, increased the nucleation time very much, indicating that the extract impeded the nucleation rate. Therefore, it can be concluded that different concentrations of *U. compressa* and *P. capillacea* algal extract increase the nucleation time and consequently retard the growth step. However, total blocking of the

electrode surface stage was not observed within the exposure period even in presence of low concentration of the extract (5 ppm), indicating that the extract can be used as a good antiscalant.

Fig. 4 shows the variation of current density after polarizing the steel electrode for 20 h in brine CaCl_2 solution, containing different concentrations of *U. compressa*, and *P. capillacea* extracts. The results indicated similar behavior for both algal extracts after addition of certain concentration of the extract, which corresponded to the initial concentration required to impede scale growth. These concentrations were up to 75 and 100 ppm for *U. compressa* and *P. capillacea* extract, respectively, indicating that lower concentration of *U. compressa* extract was sufficient to retard scale growth for a system under cathodic polarization. On the other hand, the observed final high current density of *U. compressa* algal extract indicated that higher concentrations exhibited better antiscalant properties than *P. capillacea* algal extract; since the current density has inverse relationship to the area covered by the remained nuclei. This behavior was in a good

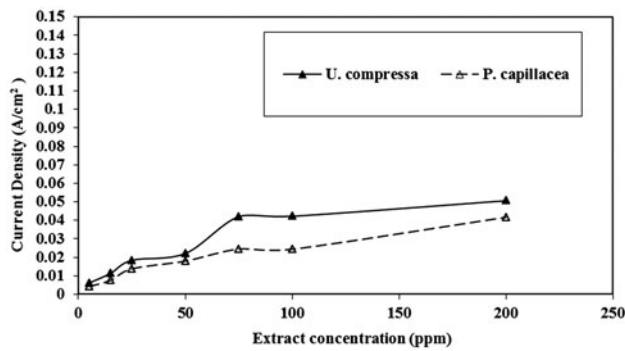


Fig. 4. Variation of current density after polarizing the steel electrode for 20 h in CaCl_2 brine solution, containing different concentrations of algal extracts.

agreement with that obtained from conductivity measurements.

3.1.2.2. *The electrochemical impedance spectra measurements.* However, several problems arise for interpreting chronoamperometry curves. First, the DC current gives only partial information on the screening effect of the insulating scale deposit on the electrode surface [26]. Second, no information was obtained about the thickness and porosity of the scale layer [29]. Accordingly, the electrochemical impedance spectra were traced during chronoamperometry measurements after 20 h without removing the working electrode from the test solution at open circuit potential to observe the nucleation, crystal growth, and total surface coverage phenomena occurring at the interface of cathodically protected steel electrode. Moreover, EIS measurements were done at rest potential for corrosion inhibition studies.

3.2. Impedance behavior at an open circuit potential in CaCl_2 brine solution

Fig. 5(a) and (b) shows the Nyquist plots, measured at an open circuit potential in a renewed CaCl_2 brine solution for the steel electrode after cathodic polarization at open circuit potential for: (a) 1 and 3 h that corresponded to crystal growth region and (b) 20 h that corresponded to total coverage of the electrode surface region.

Fig. 5(b) shows Nyquist plot measured at 1 h corresponded to nucleation region, while the plot measured at 3 h corresponded to the crystal growth region. The Nyquist plot obtained after polarizing the steel for 1 h consisted of capacitive semicircle at higher frequency region.

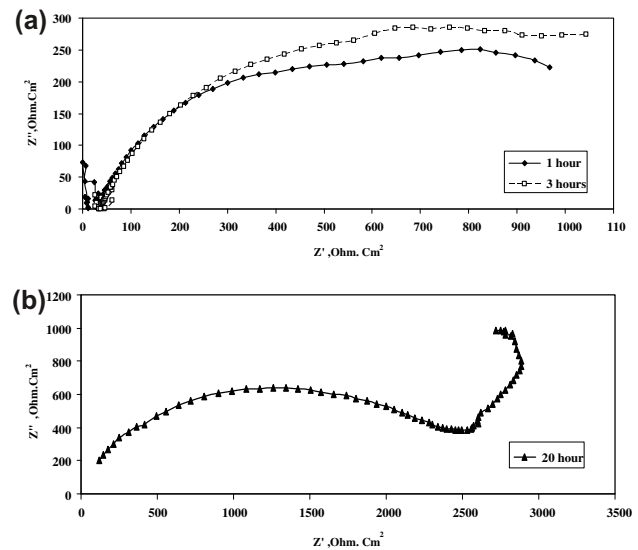


Fig. 5. (a) Nyquist plots, measured at open circuit potential in renewed CaCl_2 brine solution, for the steel electrode that was cathodically polarized in the CaCl_2 brine solution for 1 and 3 h and (b) Nyquist plots, measured at open circuit potential in renewed CaCl_2 brine solution, for the steel electrode that was cathodically polarized in the CaCl_2 brine solution for 20 h.

Fig. 5(b) shows a typical feature of depressed semi-circles followed by a low frequency tail. Lorenz and Mansfeld [30] showed similar impedance behavior for a corroding iron rotating disk electrode in a neutral aerated sodium sulfate solution.

As seen, the size of the obtained semi-circles increased with exposure time that clarifies a significant increase of steel electrode impedance. This suggests that the electrode surface has been changed by the exposure to a scaling environment due to the formation of protective scales. Moreover, it is clear that the scaling process occurs under the control of the oxygen diffusion. Therefore, a porous morphology of the scale layer can be predicted since to reduce oxygen on metal surface, the dissolved oxygen have to cross the scale layer through pores between the CaCO_3 blocks. Therefore, the increase of the electrode impedance can be attributed to the decrease of surface porosity, or in other words to the decrease of the active area due to the scale deposition that retard the penetration of the electrolyte to the metal surface and increase the charge transfer resistance.

3.2.1. Quantitative treatment

It was reported by Marín-Cruz et al. [31] that, due to the irregular form of the impedance spectra at low

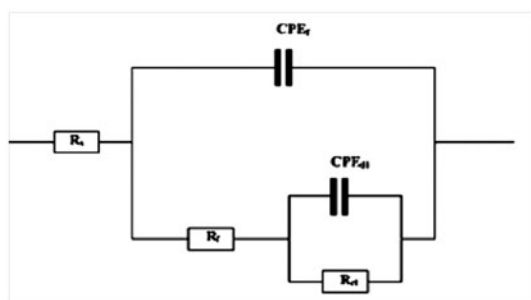


Fig. 6. Schematic for the equivalent circuit model used to determine the impedance parameters for scale process in the CaCl_2 brine solution.

frequencies, the Warburg-type diffusion must be discarded, since some authors have suggested that this irregular shape of the impedance spectra is associated to the presence of simultaneous diffusion of two species (iron ions and oxygen) through the porous surface [32]. Fig. 6 shows the equivalent circuit that was earlier proposed by Beaunier et al. [33] to fit the experimental data of impedance plots for the crystal growth regions (Fig. 5(a) and (b)), using the Gamry Echem analyst 5.3 software program. However, the analysis of diagrams was restricted to the high- and mid-frequency domains, removing the low-frequency data.

The change in the film resistance (R_f), charge transfer resistance (R_{ct}) in CaCl_2 brine solution obtained after 20 h of polarizing steel electrode at open circuit potential (vs. SCE) are given in Table 1. The data clarify that increasing exposure time increased the charge transfer and film resistances and decreased the non-ideal film, confirming the inhibitive effect of the CaCl_2 brine solution toward scales formation process. In the circuit, R_s represents the solution resistance, R_f is the resistance associated with the layer of products formed during immersion, and R_{ct} corresponds to the charge transfer resistance. CPE_f and CPE_{dl} are the constant phase elements corresponding to film and double layer capacitance.

3.3. Impedance behavior at an open circuit potential in presence of different concentrations of *U. compressa* and *P. capillacea* algal extract

Fig. 7 displays the experimentally measured impedance diagram in Nyquist format for the steel that was cathodically polarized at open circuit potential for 20 h in brine solution in the presence of different concentrations of *U. compressa* and *P. capillacea* algal extract.

Fig. 7 indicates that the scaling process in the presence of the algal extracts occurs under diffusion control. The decrease in the size of the depressed semicircles with increasing concentration of the extracts indicates the ability of the extract to impede scale formation. It was observed that increasing concentration of the extract up to 75 ppm for *U. compressa* and *P. capillacea* algal extracts slightly decreased the size of the depressed semicircle indicating that these are the critical concentration, after which insignificant increase in the inhibition efficiency of the extract to the scale formation is observed.

3.3.1. Quantitative treatment

Table 2 represents the change in the film resistance, charge transfer resistance, the non-ideal film and double layer capacitances in the presence of different *U. compressa* and *P. capillacea* algae extracts concentrations obtained after 20 h of polarizing steel electrode at -0.9 V (vs. SCE). Using Gamry Echem analyst 5.3 software to analysis the data, which clarify that increasing extract concentrations decreases the charge transfer resistance, film resistance, and increases the non-ideal film capacitance and as a result confirming the inhibitive effect of the extract toward the scale formation process. The percentage of scale inhibition can be determined from the following equation:

$$\% \text{ scale inhibition} = \frac{[(R_{ct})_0 - (R_{ct})_i]}{(R_{ct})_0} \times 100 \quad (3)$$

Table 1

Computer fit results of the impedance spectra obtained at open circuit potential for the steel electrode that was cathodically polarized for 20 h in the CaCl_2 brine solution at different time intervals

Time (h)	R_f (Ohm cm^2)	CPE_f (μF)	R_{ct} (Ohm cm^2)	CPE_{dl} (μF)	R_s (Ohm cm^2)
1	40.54	6.6	967.5	357	25.0
3	200.1	114.3	1,044	921	28.0
20	1,089	11.1	2,494	0.247	121.6

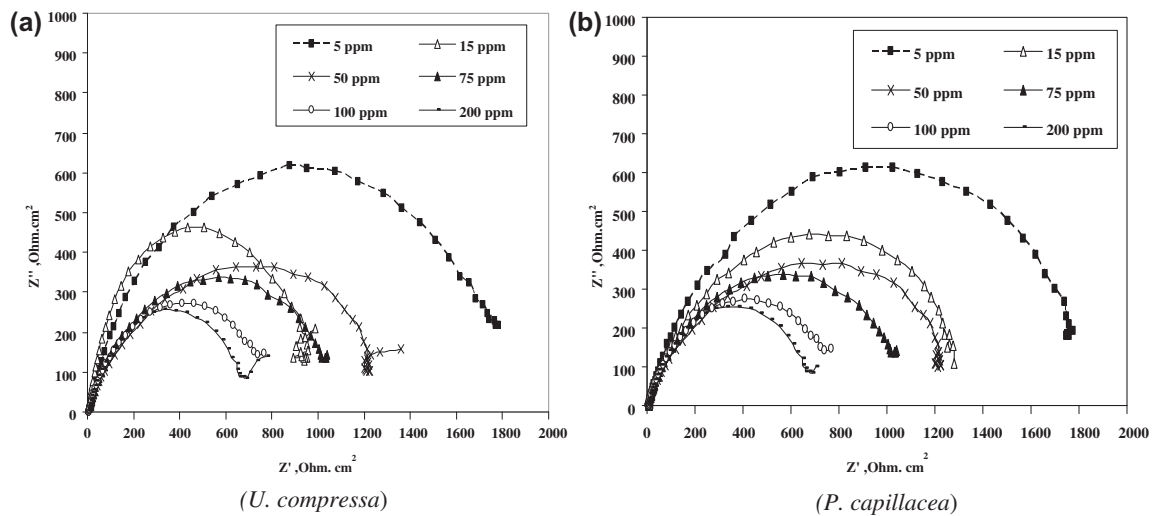


Fig. 7. Nyquist plots for steel in brine solution in the absence and presence of different concentrations of algal extract.

Table 2

Computer fit results of the impedance spectra obtained at open circuit potential for the steel electrode that was cathodically polarized for 20 h in the CaCl_2 brine solution containing different *U. compressa* and *P. capillacea* extracts concentrations

Extracts	Conc. (ppm)	R_f (Ohm cm^2)	CPE_f (μF)	R_{ct} (Ohm cm^2)	CPE_{dl} (μF)	R_s (Ohm cm^2)
<i>U. compressa</i>	5	632.0	11.74	1,771	43.14	28.6
	15	392.8	23.83	1,417	63.35	21.6
	50	281.2	36.61	1,212	88.58	15.3
	75	278.4	43.22	924.1	118.8	7.3
	100	162.4	62.75	717.4	208.0	5.3
	200	144.0	91.04	674	222.0	3.1
<i>P. capillacea</i>	5	412.8	12.35	1,853	39.85	49.6
	15	240.2	26.02	1,516	90.46	20.6
	50	263.9	39.27	1,279	89.65	11.8
	75	237.9	45.43	965.8	120.1	8.6
	100	196.4	66.93	741	175.9	4.1
	200	167.4	78.45	689.6	199.5	1.5

where $(R_{ct})_0$ and $(R_{ct})_i$ are the charge transfer resistances in the absence and presence of scale inhibitor. Fig. 8 shows the dependence of the percentage of scale inhibition on the concentration of *U. compressa* and *P. capillacea* algal extracts. The percentages of scale inhibition are 62.95 and 61.3%, respectively, in the presence of 75 ppm *U. compressa* and *P. capillacea* algal extracts. These data are in good agreement with those obtained using chronoamperometry technique.

Fig. 8 shows the dependence of the percentage of scale inhibition on the concentration of algal extract, and indicates that, the percentage of scale inhibition of *U. compressa* is higher than *P. capillacea* algal extract.

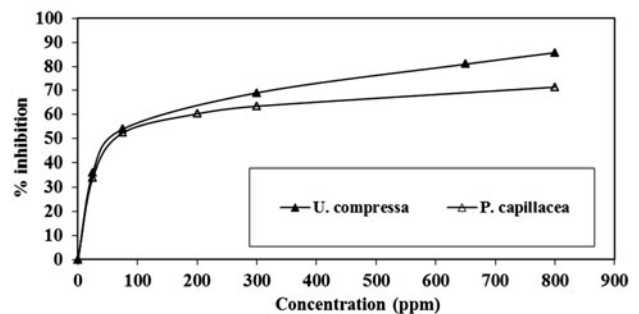


Fig. 8. Dependence of the percentage of scale inhibition on the concentrations of algal extracts.

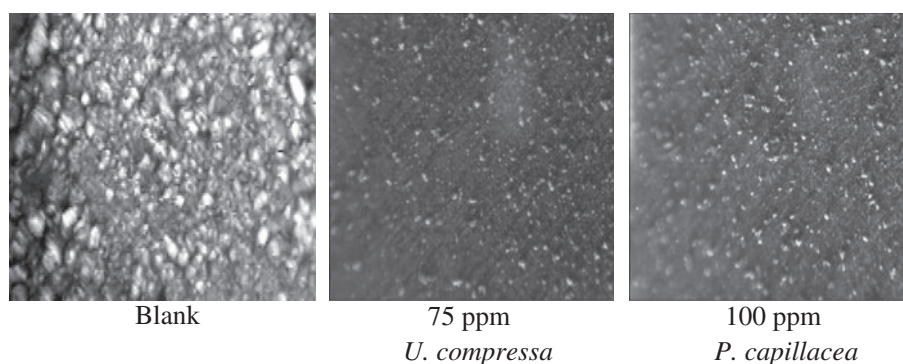


Fig. 9. Optical micrograph photo (40 \times) for cathodically polarized steel in the CaCl₂ brine solution in absence and presence of 75 ppm *U. compressa* and 100 ppm *P. capillacea* extract, respectively, after 20 h.

3.3.1.1. Optical microscopic examination. The optical micrographs of the steel electrode that was polarized at -0.9 V vs. SCE for 20 h in the CaCl₂ brine solution in the absence and presence of different algal (*U. compressa* and *P. capillacea*) extract concentrations are shown in Fig. 9. These micrographs display that, in the absence of antiscalant extracts (blank), a complete surface coverage by extremely dense scale crystals takes place that is mainly due to the fast growth rate at lower scale time. The resultant increase in the nucleation time and the accompanied decrease in the growth rate in presence of the extracts lead to decrease the amount of the scale deposited over the entire area compared to the uninhibited brine solution. The surface area occupied by the scale particles decreases with increasing antiscalant extract concentrations.

These micrographs indicate that: (i) the critical extract concentration required to inhibit scale formation is 75 and 100 ppm for *U. compressa*, and *P. capillacea* algal extract, respectively, (ii) the surface area occupied by the scale particles in presence of 75 ppm *U. compressa*, is lower than that in presence 100 ppm *P. capillacea* algal extract. These data are in good agreement with those obtained, using chronoamperometry technique.

3.3.1.2. Scanning electron microscope examinations. SEM is used to elucidate the morphology of scale formed on the surface of polarized steel electrode at -0.9 V vs. SCE for 20 h in the CaCl₂ brine solution in the absence and presence of algal (*U. compressa* and *P. capillacea*) extract concentrations.

As shown in Fig. 10(a) non-polarized steel electrode, and (b–e) calcium carbonate particles formed in the absence of scale inhibitors (blank) exhibit hexagon, rhombohedron, and two types of crystalline structure calcite (b, c), and aragonite (d, e) could be identified from these photos.

The scanning electron micrographs of the steel electrode that was polarized at -0.9 V vs. SCE for 20 h in the CaCl₂ brine solution in the presence of different algal (*U. compressa* and *P. capillacea*) extract concentrations, respectively, are shown in Fig. 11. Considering the results from SEM, the changes of scale shapes resulting from the additions of scale inhibitor show the following characteristics: (i) when scale inhibitors do not exhibit high inhibition efficiency, scale shapes are modified to a little extent; (ii) however, in the presence of scale inhibitors that exhibit high inhibition, scale shapes are completely modified and are completely different from those produced in blank solution. The already born crystal of calcium carbonate deposits lose sharp edge and exhibit high irregularity of scale morphology, such as deformed hexagon, deformed rhombohedron, fusiform, rod, disk, ball, and flower. It can be concluded that the alteration of morphology is ascribed to the change of crystal form. This may be explained on the basis that: the stabilization chemicals of the extracts absorbed onto the active sites of the growing crystals, preventing additional crystal attachment and modify the deposited scale structure. There are three stages in the crystallizing process including occurrence and disappearing of unstable phase, occurrence and disappearing of metastable phase, development of stable phase. Without scale inhibitors, metastable phases usually transform into stable phase, thus the main constitute of formed scale is calcite. When scale inhibitors are added, both formation and transformation of metastable phases are inhibited; the function of scale inhibitor is realized mainly by controlling the crystallizing process at the second stage.

3.3.1.3. Infrared examinations. Further structure analysis of the scale deposits formed on the surface of the polarized steel electrode at -0.9 V vs. SCE for 20 h in

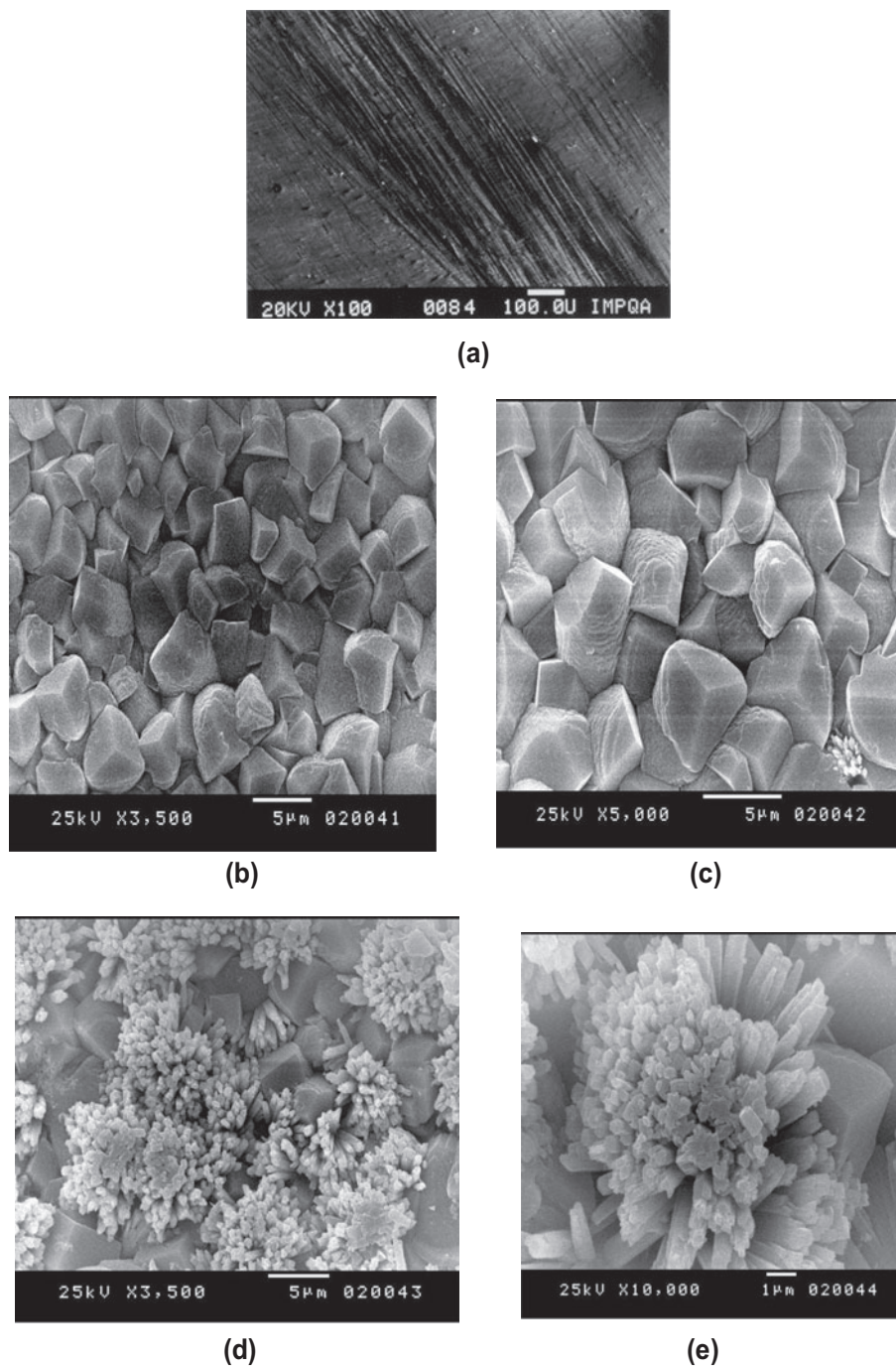


Fig. 10. SEM micrographs of (a) non-polarized steel electrode (b–e) calcium carbonate grown on the surface of polarized steel electrode at -0.9 V vs. SCE for 20 h in the CaCl_2 brine solution.

the CaCl_2 brine solution in the absence and presence of different algal (*U. compressa* and *P. capillacea*) extract concentrations was carried out using FTIR spectroscopy, as shown in Fig. 12. The spectrum of calcite (CaCO_3) is easily identified and the bands at 1,425,

876, and 712 cm^{-1} are diagnostic. The absorption at $1,425\text{ cm}^{-1}$ is due to asymmetric stretching vibration of CO_3^{2-} anion, the band at 876 cm^{-1} arises from out-of-plane bending mode, while the band at 712 cm^{-1} corresponding to in-plane bending vibrations [34].

However, in the presence of scale inhibitor, the spectrums were changed to different extent. It was found that, the intensity of peaks decreased by adding the scale inhibitor, which is fitted with the same results obtained in previous works [35,36]. This confirms the discussion presented in the scanning electron microscope part in which the scale inhibitors act as stabilizing chemicals that are absorbed onto the active sites of the growing crystals, preventing additional crystal attachment and modifying the deposited scale structure. It was found that, the intensity of peaks decreased with adding the scale inhibitor.

3.4. Corrosion inhibition

3.4.1. Electrochemical impedance spectroscopy

Fig. 13 shows Nyquist plots for steel in brine solution in the absence and presence of different algal (*U. compressa* and *P. capillacea*) extract concentrations, respectively. The impedance response consisted of distorted loop of a capacitive type whose size increases with increasing algal extract concentrations indicative of increasing inhibitive efficiency of the extract with increasing concentration.

The impedance spectra of different Nyquist plots were analyzed by fitting the experimental data to the

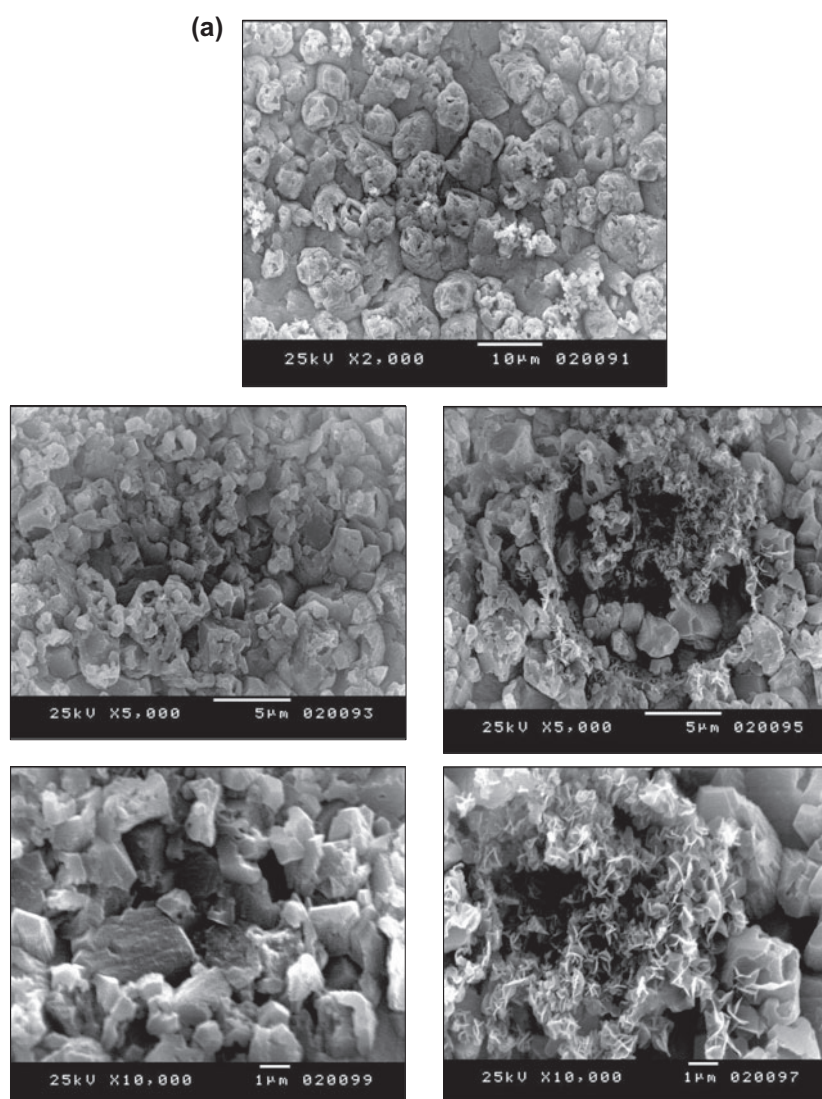


Fig. 11. (a) SEM micrographs of calcium carbonate grown on the surface of polarized steel electrode at -0.9 V vs. SCE for 20 h in the CaCl_2 brine solution in presence of 75 ppm of *U. compressa* extract and (b) SEM micrographs of calcium carbonate grown on the surface of polarized steel electrode at -0.9 V vs. SCE for 20 h in the CaCl_2 brine solution in presence of 100 ppm of *P. capillacea* extract.

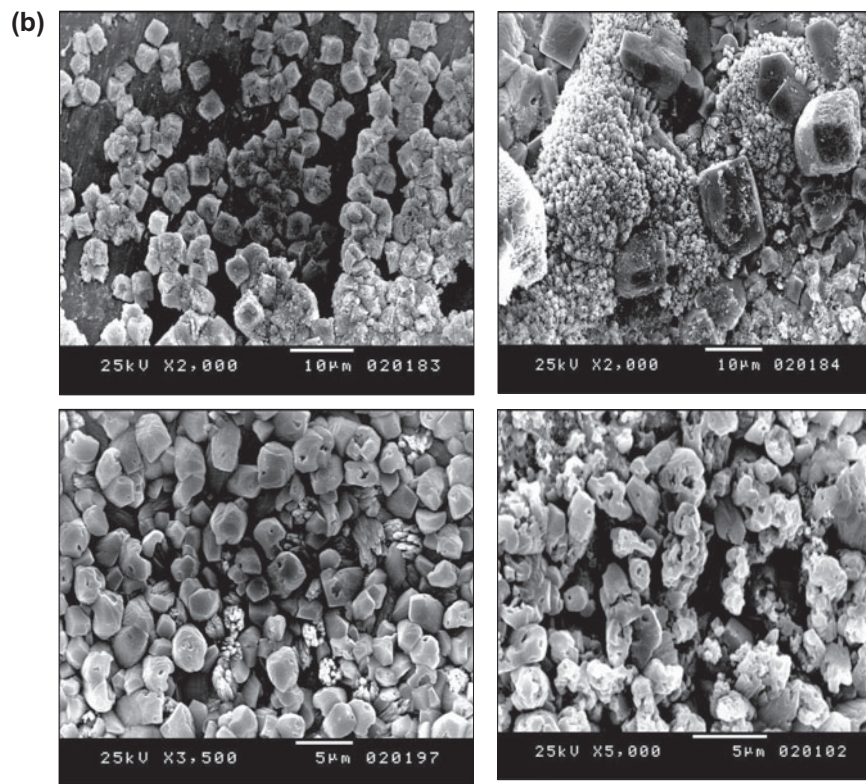


Fig. 11. (Continued).

equivalent circuit shown in Fig. 6. Computer fit results of the impedance spectra obtained in the absence and presence of different algal (*U. compressa* and *P. capillacea*) extract concentrations are given in Table 3. The data show that the charge transfer resistance increases by increasing the concentration of the extracts, which indicates that algal extracts acts as corrosion inhibitor for steel in test solution. This can be attributed to decrease in dielectric constant and/or increase in the thickness of electric double layer, suggesting that the inhibitor molecules act by adsorption mechanism at steel/solution interface.

The percentage of inhibition, % π is calculated from the following equation:

$$\% \pi = 1 - \left(\frac{R_{ct}^*}{R_{ct}} \right) \times 100 \quad (4)$$

where (R_{ct}^*) and (R_{ct}) are the charge transfer resistances with and without the corrosion inhibitor, respectively.

Fig. 14 shows the dependence of the percentage corrosion inhibition on the concentration of *U. compressa* and *P. capillacea* extracts. The percentages of corrosion inhibition are 63.2 and 62.3% in presence of 300 ppm for both types of algal extracts, respectively.

3.4.2. Potentiodynamic polarization results

Figs. 15 and 16 show the potentiodynamic polarization curves for steel in the brine solution in the absence and presence of different algal (*U. compressa* and *P. capillacea*) extract concentrations. As seen, the cathodic part of the polarization curves is characterized by a limiting current at moderate potentials indicating that the corrosion process occurs under oxygen reduction control. The displayed curves show that addition of algal extract shifts the corrosion potential (E_{corr}) to less negative values and decrease the corrosion current density (i_{corr}) indicating that the extract behaves as an anodic type inhibitor [37].

The corrosion current density was calculated from the intersection of cathodic and anodic Tafel line. The Tafel constants, β_a and β_c , were calculated as a slope of the points after corrosion potential by ± 40 mV using a computer software analysis program. The values of the electrochemical parameters for different algal (*U. compressa* and *P. capillacea*) extract concentrations are given in Table 4. The displayed data show that increasing extract concentrations decrease the corrosion current density (i_{corr}). Moreover, the anodic Tafel slopes (β_a) are approximately constant, while the cathodic Tafel slopes (β_c) have higher numerical

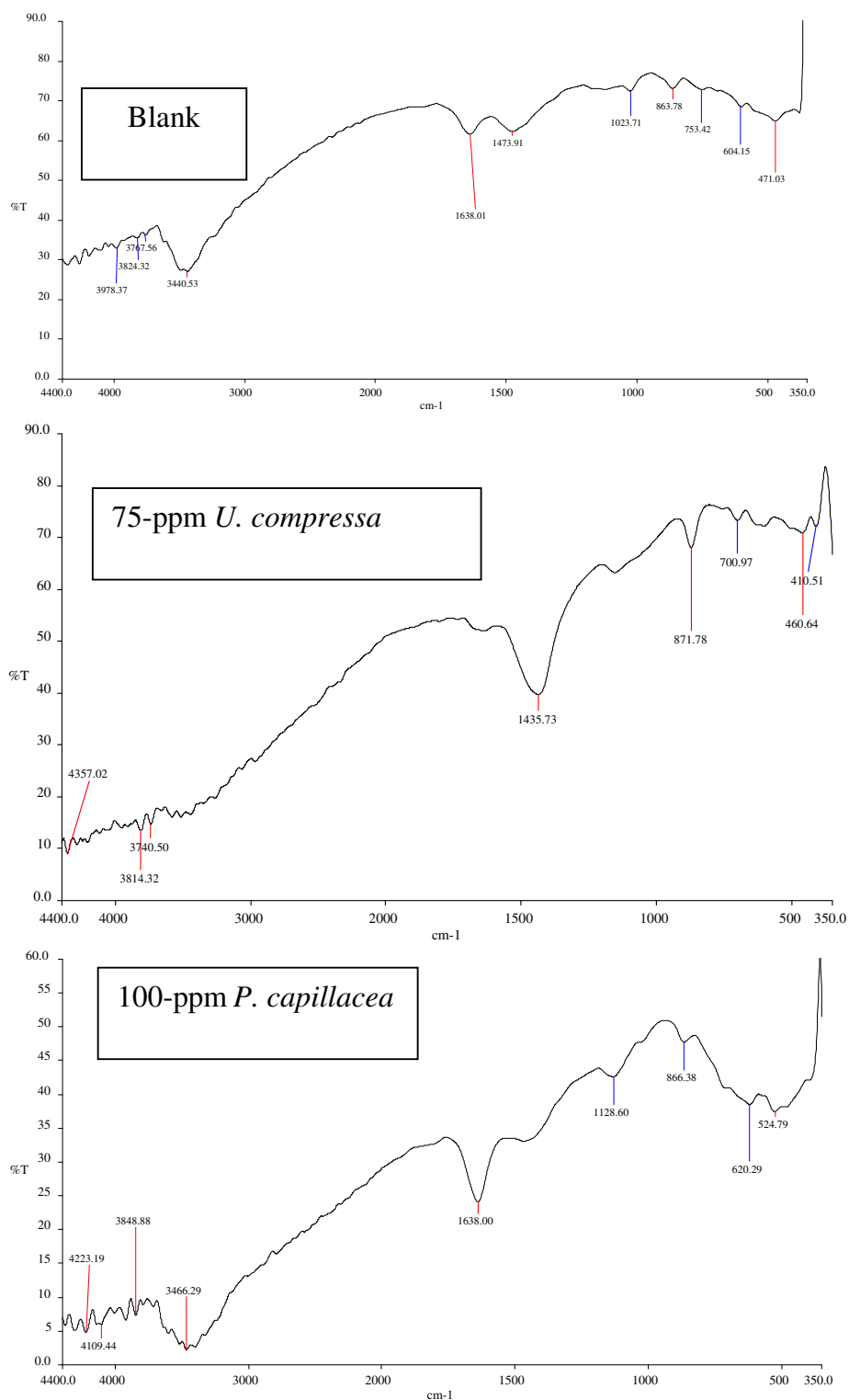


Fig. 12. IR spectra of crystalline calcium carbonate grown in the absence and presence of different *U. compressa* and *P. capillacea* algal extracts, respectively.

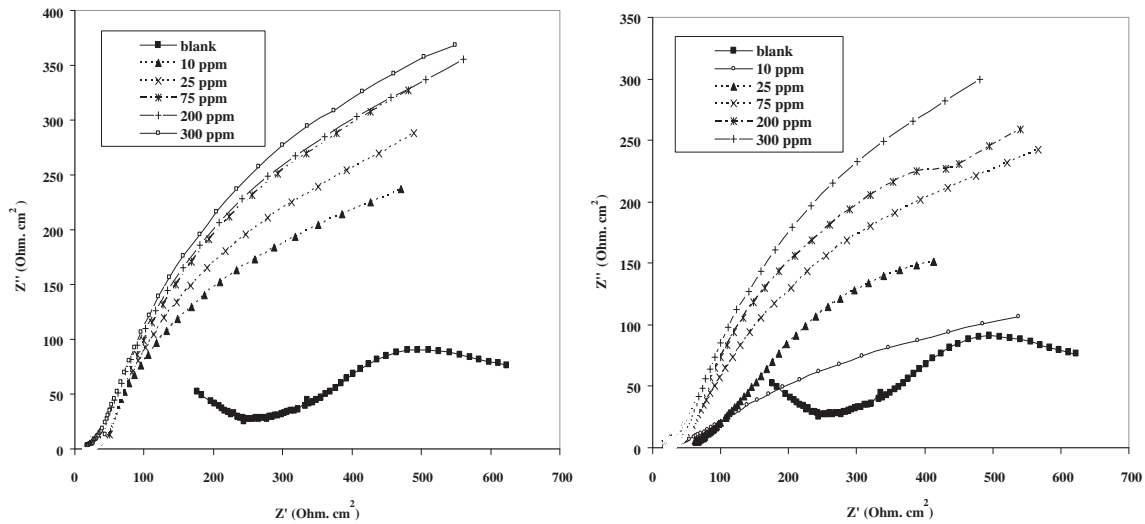


Fig. 13. Nyquist plots for steel in brine solution in the absence and presence of different concentrations of *U. compressa* and *P. capillacea* algal extracts, respectively.

Table 3

Computer fit results of the impedance spectra for steel electrode in the CaCl₂ brine solution in the absence and presence of different concentrations of *U. compressa* and *P. capillacea* extracts

	Conc. (ppm)	R _s (Ohm cm ²)	R _{ct} (Ohm cm ²)	% π
<i>U. compressa</i>	00	176.7	350	0
	10	17.8	631	60.4
	25	18.7	639	60.9
	75	22.7	642	61.1
	200	20.5	656	61.9
<i>P. capillacea</i>	300	25.1	679	63.2
	00	176.7	350	0
	10	17.2	624	59.9
	25	16.8	630	60.4
	75	20.5	639	60.9
	200	16.4	653	61.8
	300	18.3	664	62.3

values that decrease with increasing extracts concentrations suggesting that the inhibiting action of the extracts takes place by controlling the cathodic processes.

The degree of surface coverage, θ , was calculated by Tafel form:

$$\theta = [1 - (i_{corr}/i_{corr}^{\circ})] \tag{5}$$

where (i_{corr}) and (i_{corr}°) were the corrosion current densities with and without inhibitor.

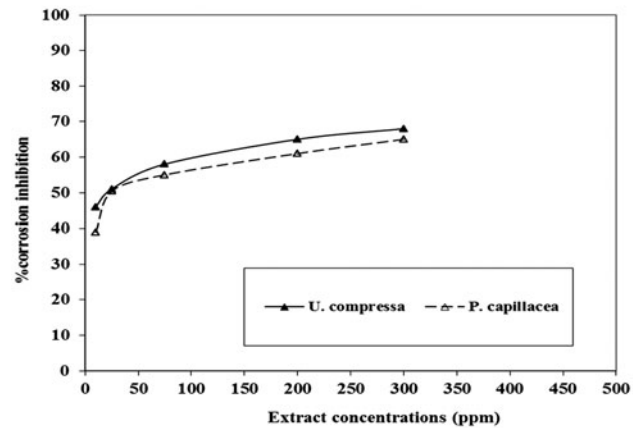


Fig. 14. Dependence of the percentage of corrosion inhibition on the concentration of algal extract.

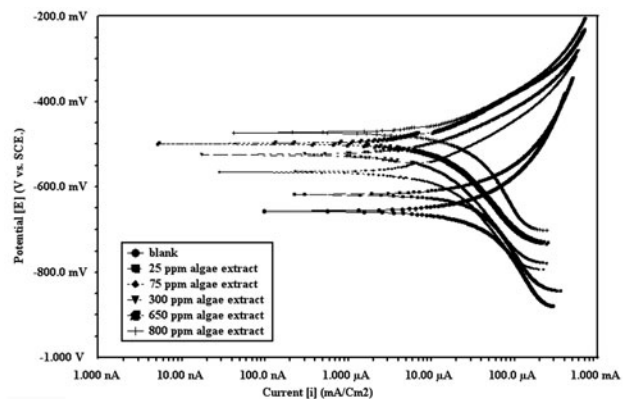


Fig. 15. Potentiodynamic polarization curves for steel in brine solution in the absence and presence of different concentrations of *U. compressa* extract.

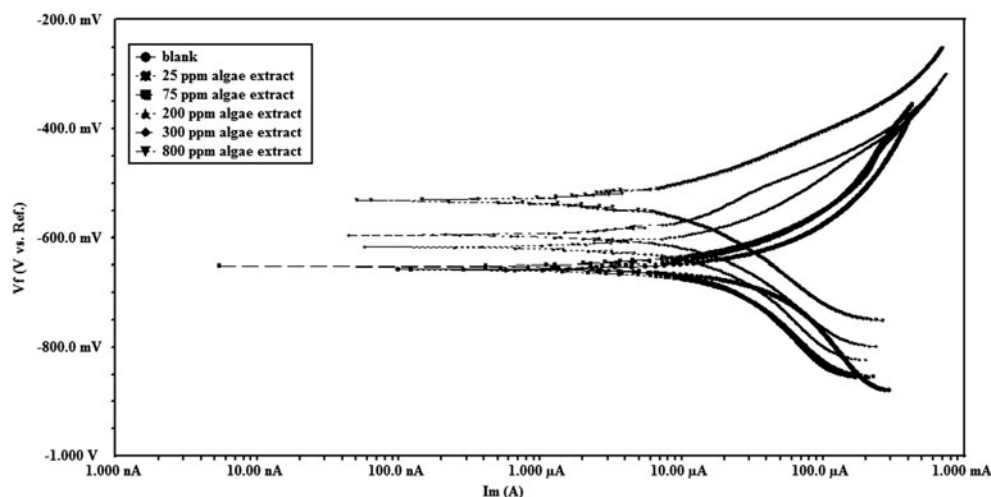


Fig. 16. Potentiodynamic polarization curves for steel in brine solution in the absence and presence of different concentrations of *P. capillacea* extract.

Table 4

Electrochemical polarization parameters of steel in brine solution in absence and presence of different concentrations of *U. compressa* and *P. capillacea* extracts

	Conc. (ppm)	(mV/decade)		$I_{\text{corr.}}$ (μA)	$-E_{\text{corr.}}$ (mV)	Corrosion rate (mpy)	θ	% π
		β_a	$-\beta_c$					
<i>U. compressa</i>	00	168	258	63	657	25.9	00	0.00
	25	130	175	40	618	23.6	0.36	36
	75	73	70	29	566	2.9	0.53	53
	300	63	86	19	525	2.6	0.69	69
	650	49	50	12	499	1.6	0.81	81
	800	55	46	9	473	1.1	0.85	85
<i>P. capillacea</i>	00	168	258	63	657	25.9	00	0.00
	25	98	199	41	628	24.4	0.34	34
	75	67	92	30	652	4.8	0.52	52
	200	64	71	25	617	3.0	0.60	60
	300	65	59	23	595	2.4	0.63	63
	800	39	42	18	532	1.8	0.71	71

The percentage of inhibition efficiency (% π) was calculated either from the degree of surface coverage:

$$\% \pi = \theta \times 100 \quad (6)$$

where % π , i_o , and i are the percentage of inhibition efficiency and the corrosion current density, in the absence and presence of different concentrations of extracts, respectively.

The good inhibiting action of *U. compressa* and *P. capillacea* algal extracts at high concentrations. Furthermore, it can be seen that usually when the concentration of *U. compressa* and *P. capillacea* algae extracts

increased, the inhibition efficiencies increased reaching values of 69 and 63.4%, at 300 ppm *U. compressa* and *P. capillacea* extracts, respectively, that is fitting with the same results obtained previously.

Fig. 17 shows the variation of the percentage of inhibition for algal (*U. compressa* and *P. capillacea*) extracts. Results of the inhibition efficiencies revealed that: It can be seen that usually when the concentration of *U. compressa* and *P. capillacea* algal extracts increased, the degree of surface coverage (θ) increased reaching values of 0.69 and 0.63 at 300 ppm *U. compressa* and *P. capillacea* algal extracts, respectively. These data are in good agreement with the results obtained from the

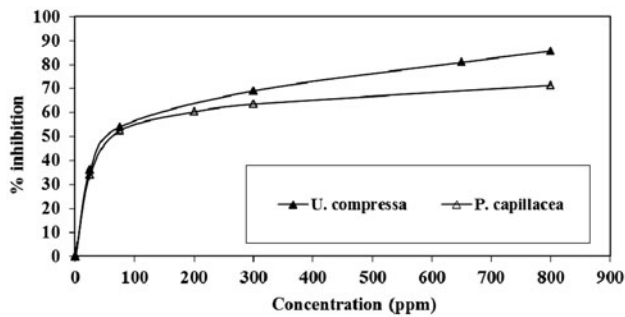


Fig. 17. The variation of the percentage of corrosion inhibition with *U. compressa* and *P. capillacea* extracts concentrations.

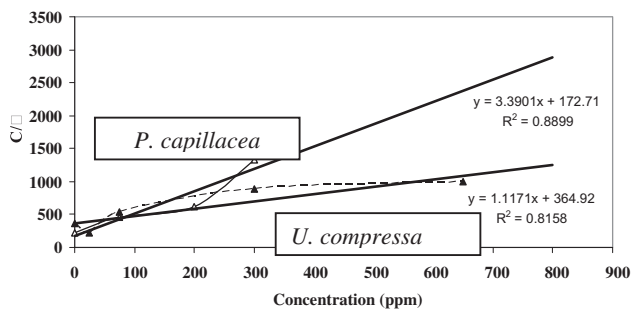


Fig. 18. Langmuir isotherm curve for different *U. compressa* and *P. capillacea* extracts concentrations.

variation of the percentage of inhibition with algal extract concentrations.

3.4.3. Langmuir isotherm results

Several adsorption isotherms were attempted to fit θ values including that of Frumkin, Temkin, Freundlich, and Langmuir isotherm. However, the best fit was obtained by assuming the Langmuir isotherm. The strong correlation ($R^2 = 0.999$) of the Langmuir isotherm was obtained, while the correlations of other isotherms was less than 0.9. The Langmuir isotherm is given by [38]:

$$\frac{C}{\theta} = C + \left(\frac{1}{K}\right) \quad (7)$$

where C is the concentration of inhibitor, θ is the fractional surface coverage, and K is the adsorption equilibrium constant.

Fig. 18 shows Langmuir isotherm curve, where adsorption equilibrium constant K can be detected from the intercept of the Langmuir isotherm curve.

The data show that K equals 0.87 and 0.82 for *U. compressa* and *P. capillacea* extracts, respectively. The high value of K for studied inhibitors indicates stronger adsorption on the metal surface in calcium chloride brine solution with different concentrations of inhibitors, which is fitting with the same results obtained latter [39]. The data indicate that: (i) K of *U. compressa* is higher than *P. capillacea* extracts; (ii) *U. compressa* has a higher value of K for studied inhibitors indicate stronger adsorption on the metal surface in calcium chloride brine solution with different concentrations of inhibitors. On the other hand, *P. capillacea* has a lower value of K studied inhibitor indicates weaker adsorption on the metal surface in calcium chloride brine solution with different concentrations of inhibitors.

4. Conclusions

- (1) This paper has mainly explored the possibility for some natural products to act as antiscalant and anticorrosion inhibitors in cooling systems used in pharmaceutical and food industries.
- (2) (*U. compressa* and *P. capillacea*) extracts could act efficiently as antiscalant preventing the deposition of CaCO_3 as well as retarding the corrosion of steel.
- (3) The formation of a protective layer of scales is always accomplished by characteristic spectral changes and a rapid change in electrode impedance.
- (4) Electrochemical techniques confirmed that the addition of algal extracts to the brine solution even in low concentrations prevents total coverage of the electrode surface stage with scale indicating that these extracts act as good antiscalant.
- (5) The microscopic examinations explained that, the alteration of morphology is ascribed to the change of crystal form.
- (6) Potentiodynamic polarization measurements and EIS indicated that algal extracts inhibit the corrosion of steel in the alkaline brine solution, i.e. both extracts have a dual function effect as antiscalant for CaCO_3 deposit and as corrosion inhibitor for steel in alkaline CaCl_2 brine solution simulating the treatment of cooling plants.
- (7) No reference to the use of algae as a corrosion and scale inhibitor has been found in literature: it is thus believed to represent a potentially new, environmentally safe inhibitor suitable for treating cooling water systems.

References

- [1] D. Zeng, W. Qin, Study on a novel composite eco-friendly corrosion and scale inhibitor for steel surface in simulated cooling water, *Surf. Eng. Mat. Adv. Technol.* 2 (2012) 137–141.
- [2] C.A. Grillo, M.V. Mirífico, M.L. Morales, M.A. Reigosa, M.F. Lorenzo de Mele, Assessment of cytotoxic and cytogenetic effects of a 1, 2, 5-thiadiazole derivative on CHO-K1 cells. Its application as corrosion inhibitor, *J. Hazard. Mater.* 170 (2009) 1173–1178.
- [3] M. Chaussemier, E. Pourmohtasham, D. Gelus, N. Pécoul, H. Perrot, J. Lédion, H. Cheap-Charpentier, O. Horner, State of art of natural inhibitors of calcium carbonate scaling. A review article, *Desalination* 356 (2015) 47–55.
- [4] H.K. Can, G. Üner, Water-soluble anhydride containing alternating copolymers as scale inhibitors, *Desalination* 355 (2015) 225–232.
- [5] Y.M. Al-Roomi, K.F. Hussain, Application and evaluation of novel acrylic based CaSO_4 inhibitors for pipes, *Desalination* 355 (2015) 33–44.
- [6] A. Rochdi, R. Touir, M. El Bakri, M. Ebn Touhami, S. Bakkali, B. Mernari, Protection of low carbon steel by oxadiazole derivatives and biocide against corrosion in simulated cooling water system, *J. Environ. Chem. Eng.* 3 (2015) 233–242.
- [7] F. Liu, L. Zhang, X. Yan, X. Lu, Y. Gao, C. Zhao, Effect of diesel on corrosion inhibitors and application of bio-enzyme corrosion inhibitors in the laboratory cooling water system *Corros. Sci.* 93 (2015) 293–300
- [8] A.C. Bastos, M.G. Ferreira, A.M. Simões, Corrosion inhibition by chromate and phosphate extracts for iron substrates studied by EIS and SVET, *Corros. Sci.* 48 (2006) 1500–1512.
- [9] D. Lisitsin, Q. Yang, D. Hasson, R. Semiat, Inhibition of CaCO_3 scaling on RO membranes by trace amounts of zinc ions, *Desalination* 183 (2005) 289–300.
- [10] D.-J. Choi, S.-J. You, J.-G. Kim, Development of an environmentally safe corrosion, scale, and microorganism inhibitor for open recirculating cooling systems, *Mater. Sci. Eng. A* 335 (2002) 228–235.
- [11] A.M. Abdel-Gaber, B.A. Abd-El-Nabey, E. Khamis, D.E. Abd-El-Khalek, Investigation of fig leaf extract as a novel environmentally friendly antiscalant for CaCO_3 calcareous deposits, *Desalination* 230 (2008) 314–328.
- [12] A.M. Abdel-Gaber, B.A. Abd-El-Nabey, E. Khamis, D.E. Abd-El-Khalek, A natural extract as scale and corrosion inhibitor for steel surface in brine solution, *Desalination* 278 (2011) 337–342.
- [13] A.M. Abdel-Gaber, B.A. Abd-El-Nabey, E. Khamis, H. Abd-El-Rhmann, H. Aglan, A. Ludwick, Green antiscalant for cooling water systems, *Int. J. Electrochem. Sci.* 7 (2012) 11930–11940.
- [14] E.M.E. Mansour, A.M. Abdel-Gaber, B.A. Abd-El-Nabey, N. Khalil, E. Khamis, A. Tadros, H. Aglan, A. Ludwick, Developing and testing of a new anticorrosive coating containing algae as natural inhibitor for preventing marine corrosion of steel, *Corrosion* 59 (2003) 242.
- [15] B. Santelices, M. Hommersand, *Pterocladia*, a new genus in the Gelidiaceae (Gelidiales, Rhodophyta), *Phycologia* 36(2) (1997) 114–119.
- [16] A. Holzinger, K. Herburger, F. Kaplan, L.A. Lewis, Desiccation tolerance in the chlorophyte green alga *Ulva compressa*: Does cell wall architecture contribute to ecological success? *Planta* 242 (2015) 477–492.
- [17] G.F. El-Said, A. El-Sikaily, Chemical composition of some seaweed from Mediterranean Sea coast, Egypt, *Environ. Monit. Assess.* 185 (2013) 6089–6099.
- [18] G. Jiao, G. Yu, J. Zhang, H. Ewart, Chemical structures and bioactivities of sulphated polysaccharides from marine algae, *Mar. Drugs* 9 (2011) 196–223.
- [19] W. Wang, S.-X. Wang, H.-S. Guan, The antiviral activities and mechanisms of marine polysaccharides: An overview, *Mar. Drugs* 10 (2012) 2795–2816.
- [20] E.L. McCandless, J.S. Craigie, Sulphated polysaccharides in red and brown algae, *Plan* 112 (1979) 201–212.
- [21] A. Hardisson, I. Frias, A. de Bonis, G. Lozano, A. Báez, Mercury in algae of the Canary Islands littoral, *Environ. Int.* 24(8) (1998) 945–950.
- [22] A.A. Aleem, The marine algae of Alexandria, Privately published, Egypt, 1993, 139 pp.
- [23] I. Dreła, P. Falewicz, S. Kuczkowska, New rapid test for evaluation of scale inhibitor, *Water Res.* 32(88) (1988) 31–32.
- [24] S. Zielinski, Scientific Papers of the Institute of Inorganic Technology, Monographs, Technical University of Wroclaw, Poland, 20, 1981.
- [25] D. Schweinsberg, G. George, A. Nanayakkawa D. Steinert. The protective action of epoxy resins and curing agents—Inhibitive effects on the aqueous acid corrosion of iron and steel, *Corros. Sci.* 28 (1988) 33–42.
- [26] C. Gabrielli, M. Keddama, A. Khalil, R. Rosset, M. Zidoune, Study of calcium carbonate scales by electrochemical impedance spectroscopy, *Electrochim. Acta* 42(8) (1997) 1207–1218.
- [27] C. Deslouis, D. Festy, O. Gil, V. Maillot, S. Touzain, B. Tribollet, Characterization of calcareous deposits in artificial sea water by impedances techniques: 2-deposit of $\text{Mg}(\text{OH})_2$ without CaCO_3 , *Electrochim. Acta* 45(11) (2000) 1837–1845.
- [28] J.-F. Yan, R.E. White, R.B. Griffin, parametric studies of the formation of calcareous deposits on cathodically protected steel in seawater, *J. Electrochem. Soc.* 140 (1993) 1275.
- [29] M. Sfaira, A. Srhiri, M. Keddama, H. Takenouti, Corrosion of a mild steel in agricultural irrigation waters in relation to partially blocked surface, *Electrochim. Acta* 44 (1999) 4395–4402.
- [30] W.J. Lorenz, F. Mansfeld, Interface and interphase corrosion inhibition, *Electrochim. Acta* 31(4) (1986) 467–476.
- [31] J. Marín-Cruz, R. Cabrera-Sierra, M.A. Pech-Canul, I. González, EIS study on corrosion and scale processes and their inhibition in cooling system media, *Electrochim. Acta* 51(8–9) (2006) 1847–1854.
- [32] J.L. Dawson, D.G. John, Diffusion impedance—An extended general analysis, *J. Electroanal. Chem. Interfacial Electrochem.* 110 (1980) 37.
- [33] L. Beaunier, I. Epelboin, J.C. Lestrade, H. Takenouti, Etude électrochimique et par microscopie électronique a balayage, du fer recouvert de peinture (Electrochemical study and scanning electron microscopy of iron coated with paint), *Surf. Technol.* 4 (1976) 237–254.

- [34] G.E. Christidis, European mineralogical union notes in mineralogy, Mineral. Soc. Great Britain and Ireland 9 (2011) 213.
- [35] G.C. Zhang, J.J. Ge, M.Q. Sun, B.L. Pan, T. Mao, Z.Z. Song, Investigation of scale inhibition mechanisms based on the effect of scale inhibitor on calcium carbonate crystal forms, *Sci. China Series B: Chem.* 50(1) (1976) 114–120
- [36] A.C. Tas, Monodisperse calcium carbonate microtablets forming at 70°C in prerrefrigerated CaCl₂-gelatin-urea solutions, *Int. J. Appl. Ceram. Technol.* 6(1) (2009) 53–59.
- [37] M.N. El-Haddad, Chitosan as a green inhibitor for copper corrosion in acidic medium, *Int. J. Biol. Macromol.* 55 (2013) 142–149.
- [38] I. Langmuir, The constitution and fundamental properties of solids and liquids. Part I. Solids, *J. Am. Chem. Soc.* 38 (1916) 2221.
- [39] J. Bessone, C. Mayer, K. Jüttner, W.J. Lorenz, AC-impedance measurements on aluminium barrier type oxide films, *Electrochim. Acta* 28 (1983) 171.